Combined Field and Structure from Motion Survey to Identify Rock Discontinuity Sets of Aa Shallow Rockslide

Combined Field and Structure from Motion Survey to Identify Rock Discontinuity Sets of Aa Shallow Rockslide

Alberto Bolla [1], Alberto Beinat [2], Paolo Paronuzzi [1], Chiara Peloso [2]

[1] Polytechnic Department of Engineering and Architecture, University of Udine, via Cotonificio 114, 33100 Udine, Italy
[1] Polytechnic Department of Engineering and Architecture, University of Udine, via delle Scienze 206, 33100 Udine, Italy

alberto.bolla@uniud.it

Abstract. The present work shows the results of a combined field and Structure from Motion (SfM) survey performed on the detachment surface of a shallow rockslide that occurred in the Rosandra Valley (Trieste, NE Italy), which was aimed at testing the use of 3D models obtained from Remote Sensing (RS) techniques to identify joint sets affecting unstable rock masses. According to discontinuity orientation data acquired from the field (N = 223), the investigated rock mass is affected by at least nine joint sets characterised by a notable variability. The extraction of joint sets from the 3D point cloud representing the surveyed rock outcrop was strongly sensitive to the point cloud density and the values of the controlling parameters of the density function embedded within the discontinuity extractor. This work demonstrates that, in order to properly identify rock joint sets, the exclusive application of a RS approach cannot fully substitute the traditional field survey, and the estimation of discontinuity sets should be integrated with joint orientation data acquired using a geological compass. To maximise its capabilities, the semi-automatic discontinuity set extraction from 3D point clouds should always be supported by a significant statistical sample of joint orientation measurements that are preliminarily collected from the field.

1. Introduction

Rock slope failures are controlled by a number of factors, including the degree of fracturing of the rock mass involved in the rupture and the specific orientation of the geological discontinuities within the rock mass among others. However, rock joints have variable geometrical characteristics, basically depending on their specific origin [1]. Pre-existing joints of tectonic origin are commonly more persistent, with surfaces of highly variable areas (from dm^2 up to tens or hundreds of m^2), and can also be undulated, with notable variability in their mean orientation. Differently, gravity-induced joints [1–3] that affect unstable slopes subjected to a progressive failure mechanism [4, 5] are characterised by irregular surfaces of small areas (in the order of cm^2 or dm^2). These newly formed cracks, which are related to the rupture of rock bridges and other intact rock parts [6–8], can have the same orientation of pre-existing joints or, in some circumstances, show a different attitude, possibly resulting in additional joint sets [2, 3]. Owing to their lower extent compared with pre-existing tectonic joints [1, 9], gravity-induced cracks often remain undetected. The aforementioned issues demonstrate that proper identification of the discontinuity sets affecting a rock slope susceptible to failure is mandatory to predict the potential failure mechanism, the unstable volume and the related slope stability condition.

In common practice of rock mechanics, discontinuity sets affecting a rock mass are recognised on the basis of a representative statistical sample of joint orientation measurements acquired from the field using a traditional geological compass. However, field surveys may result as time consuming, and in some circumstances, operative conditions can be dangerous due to possible block collapses or not feasible due to inaccessible or highly vertically extended outcrops. To overcome these critical issues, newly developed study approaches agree on integrating or even replacing field measurements directly acquired from the rock outcrop with joint orientation data extracted from a 3D high-resolution digital representation of the investigated outcrop [10–12]. This approach has two fundamental stages that are functionally connected. In the first stage, a sufficiently precise, complete and detailed 3D digital model is produced in the form of a dense point cloud by means of modern Remote Sensing (RS) survey techniques. In the second stage, orientation data of rock planes is semi-automatically extracted from the dense point cloud representing the surveyed outcrop by using a specific software for the structural analysis of the rock mass. Among the various RS techniques, the Structure from Motion (SfM), an automated photogrammetric technique based on computer vision algorithms, is increasingly used to reconstruct 3D high-resolution virtual models of rock outcrops with the aim of identifying rock joint sets affecting the surveyed rock mass [13, 14].

However, discontinuity sets extracted from point clouds are rarely compared with a significant statistical sample of joint orientation measurements directly acquired from the field [14, 15]. This prevents thorough awareness of the strengths, and especially, of the drawbacks in the use of 3D digital models produced by RS techniques to analyse the structural arrangement of rock masses. To address this issue, the present work shows the results of a combined field and SfM survey performed on the detachment surface of a shallow rockslide that occurred in the Rosandra Valley (Trieste, NE Italy; figure 1), which was aimed at testing the use of 3D models obtained from RS techniques to identify joint sets affecting unstable rock masses.

2. RS techniques for outcrop modelling and discontinuity extraction solutions

In the past, the only viable solution for the production of 3D high-resolution models was offered by the traditional terrestrial photogrammetric technique. This approach required the employment of special metric or semi-metric cameras, and a laboratory intensive manual stereo restitution by way of dedicated analytical or digital stereo plotters. Besides the need for expensive instruments and specific operator skills, other drawbacks were the relatively low detail of the geometric features surveyed and the limited processing and analysing support offered by the computers at that time. Innovations in the geomatic field that occurred in the last two decades led to the development and diffusion of two efficient survey techniques — terrestrial laser scanning (TLS) and Structure from Motion (SfM) photogrammetry — capable of providing 3D high-resolution and high-accuracy digital representations of the surveyed outcrop. TLS techniques were the first to be tested for this purpose and are still largely employed [e.g. 16, 17]. Current instruments are commonly capable of recording up to several hundred thousand points per second, with a sample distance that can reach a few millimetres and with an accuracy of less than one centimetre. As these are active devices, TLSs are unaffected by illumination condition, and their operative range can reach several thousand meters. In contrast, this technique have some notable limitations: instrument equipment is still rather bulky and expensive; point density is variable, as a function of the point distance and of the relative exposition of the object surface; obstacles and occlusion along the line of sight can hide significant portions of the surface leading to holes in the 3D model; for large and complex outcrops, the full scan is obtained through a careful co-registration of various partial clouds taken from different locations.

SfM is a recent photogrammetric range imaging technique developed in the computer vision community. Although essentially based on the classical stereoscopic principles, thanks to its efficient image matching approach, it has the ability to estimate camera positions and orientations automatically without needing to establish an extensive ground control point (GCP) network. After pose estimation, automatic, computer intensive, multi-view stereo matching provides a geometric representation of the object in the form of a dense 3D point cloud, in the same way as a TLS, but textured. The images can

be acquired with a consumer-level digital camera, not necessarily metric, the essential rule is to have multiple, redundant, overlapping photographs of the object, taken from different points. SfM being a passive technique, it requires good photographic conditions, adequate illumination, radiometry and resolution. Furthermore, the objects must have a variegated texture. If there is no chromatic variation on the surfaces, correspondences between homologous pixels cannot be established and the photogrammetric restitution fails. In case of large, dangerous or difficult to access rock walls, it is common practice to install a camera aboard a UAV and safely obtain full photographic coverage of the object. Thanks to its instrumental and operational advantages, and the availability of low-cost high-resolution cameras and drones, SfM has gained wide popularity in geosciences, forestry, archaeology and cultural heritage as a cheaper and superior alternative to TLS.

The RS approach requires the analysis of the 3D model to identify discontinuity parameters. This represents a critical step, which still attracts research efforts with the aim of identifying an optimal solution. As a consequence, tens of automatic or semi-automatic approaches exist with their own strengths and limitations (see [18] for an updated critical review of the proposed discontinuity extraction methods). Besides manual visual delineation of the outcrop parameters carried out in the laboratory [10], the various solutions essentially differ on the basis of the 3D model structure considered, point cloud vs. triangular mesh, and on the strategy adopted to outline small regions of coplanar points, e.g. k-means clustering vs. seeded region growing, by way of their orientation parameters (normal vector and curvature). Semi-automatic solutions generally perform better, but depend on one or more working parameters (e.g. k-NN search value for point orientation estimation, number of classes of K-means, etc.), which must be provided by the user and carefully tuned on the basis of a representative subset manually derived by the 3D model or directly observed in the field.

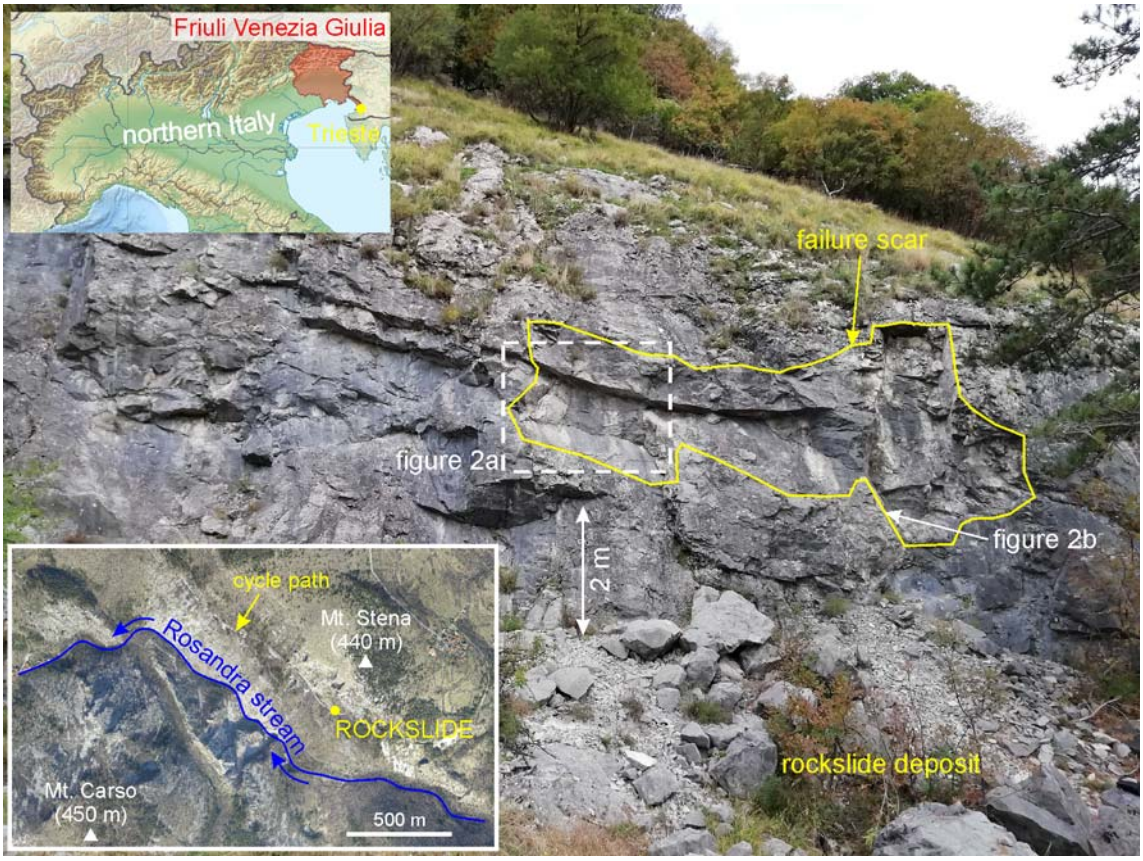

Figure 1. The investigated shallow rockslide in the Rosandra Valley (NE Italy), which involved a 6 m high re-profiled limestone scarp overlooking a cycle path.

3. The investigated rock slope failure

The rockslide investigated occurred in March 2004 in the Rosandra Valley, near the town of Trieste (north-eastern Italy), and involved a 6 m-high re-profiled limestone scarp overlooking a cycle path (figure 1). The failed rock volume has been estimated to be 6–7 m^3. The shallow rockslide was caused by freeze-thaw cycles and mobilised a number of rock blocks that propagated for a short distance and stopped on the underlying gentle slope close to the cycle path. The failure surface can be subdivided into adjacent source areas that are associated with the parallelepiped and polyhedral blocks involved in the slope collapse. The failure kinematism of the blocks was characterised by planar sliding or mixed sliding/toppling. Field observations ascertained that the slope failure occurred as a result of the progressive rupture of a number of rock bridges, thus highlighting a progressive failure mechanism (figure 2a). The identified failed rock bridges have areas ranging from 70–80 cm^2 up to 400–500 cm^2, i.e. they are small when compared with the total extent of the detachment planes that bounded the collapsed blocks. The specific location of the failed rock bridges demonstrates that the slope failure was characterised by a multistage process in which the adjacent rock blocks quickly collapsed in a sequential manner. In fact, the slope failure was enabled by the progressive rupture of the rock bridges, where stress concentrations overcame the intact rock strength, thus causing their rupture and the ensuing block collapse. Observations acquired from the rock scarp testify to the presence of newly formed fractures caused by gravitational processes that are the result of intact rock rupture related to the slope progressive failure mechanism. These gravity-induced cracks delimit a number of unstable blocks susceptible to failure and are recognisable on the field as very irregular (zigzag) fractures that penetrate into the rock mass and are characterised by variable joint openings (figure 2a, b).

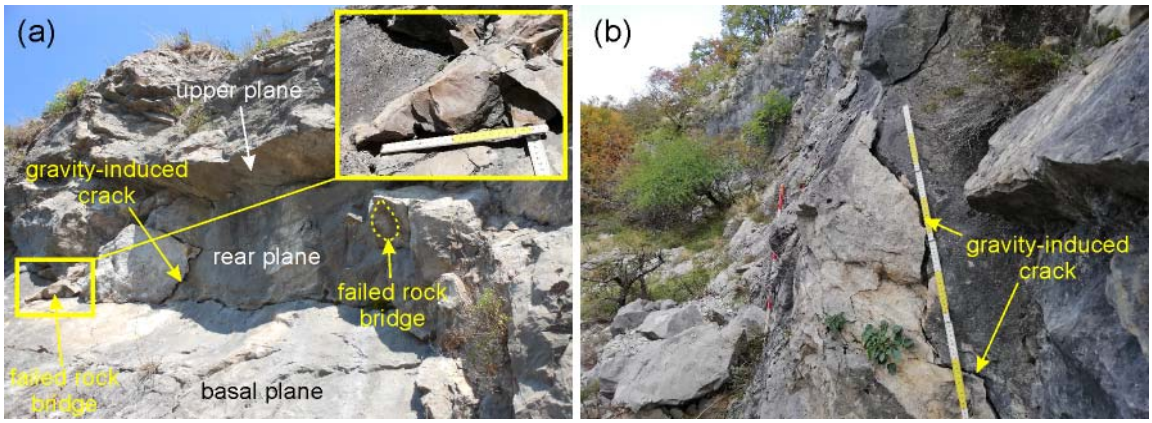

Figure 2. (a) The left sector of the failure scar showing the main detachment planes and two failed rock bridges. Note the gravity-induced crack that bounds an unstable block susceptible to failure. (b) Detail of a gravity-induced crack affecting the rock mass in the central-right sector of the failure scar.

3.1. Measured joint orientation data

Joint orientation data was collected from the field through a traditional geological compass. The large amount of field measurements (N = 223) represents a significant statistical sample of rock discontinuities that helps define the structural arrangement of the rock mass. The joint sets have been identified on the basis of the pole plot distribution and considering relative frequencies of clusters higher than 3%. As a result, at least nine rock joint sets have been identified (figure 3a). This considerable number of discontinuity sets reflects a complex tectonic framework of the Rosandra Valley and is common for sedimentary rock masses in Alpine geological contexts [3]. When considering the detachment planes of the rockslide, set J1 includes the basal sliding planes, set J3 contains the rear release planes of the collapsed blocks, and sets J4 and J5 include the lateral release planes. Joint set J2 contains low-angle bedding planes and overthrust surfaces that represent the upper detachment planes of the failed blocks. Joint sets J1–J3 are characterised by a high variability (figure

3b), which reflects slight differences in the attitude of the persistent and curvilinear bedding planes and overthrust surfaces over various areas of the failure surface. Sets J1 and J3 are the clusters with the highest relative frequency among the measured joints (figure 3b). In the stereographic projection of figure 3a, the poles to plane of some detected gravity-induced cracks have been reported. Some of these newly formed fractures belong to the previously identified joint sets, suggesting that cracks caused by gravity have the same orientation as pre-existing tectonic joints. In some cases, poles to planes of gravity-driven joints are not included within the identified joint sets, showing a different attitude compared with pre-existing joints. Therefore, on the basis of the field measurements, no additional joint sets of gravitational origin alone can be recognised.

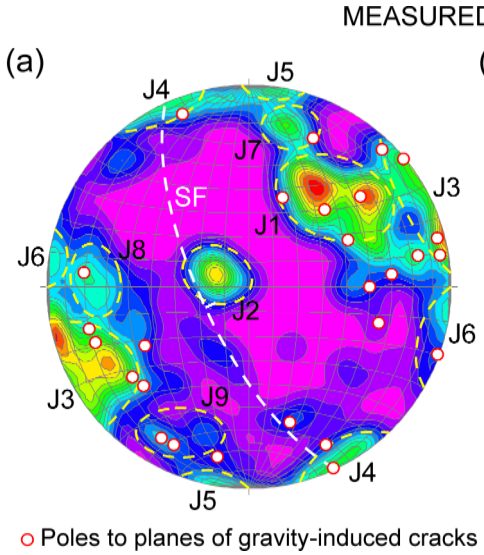

(b)

Joint set	Dip dir. [N°E] mean ± st.dev.	Dip [°] mean ± st.dev.	Relative frequency [%]
J1	227 ± 15	54 ± 09	21.5
J2	109 ± 20	14 ± 07	6.3
J3	063 ± 11	79 ± 10	23.3
J4	338 ± 10	84 ± 04	8.5
J5	188 ± 06	85 ± 07	4.9
J6	282 ± 09	85 ± 05	5.4
J7	194 ± 04	70 ± 04	3.6
J8	095 ± 08	66 ± 07	5.8
J9	025 ± 08	71 ± 07	3.6

Figure 3. (a) Contour pole plot (Schmidt stereonet, lower hemisphere) of rock discontinuities measured on the investigated limestone scarp. The orientations of the slope face (SF) and of the gravity-induced cracks are also shown. (b) Orientation data of measured joint sets.

4. Photogrammetric survey of the rock outcrop

The irregular morphology and low height of the surveyed rock scarp were key factors for the adoption of the SfM technique. Indeed, to avoid gaps in the 3D model despite the limited extension of the rock wall (27 m^2), TLS would have required scans from different locations and a consequent co-registration of the obtained partial models. The images needed for the photogrammetric survey were taken from the ground, in about 45 minutes, with a Nikon Coolpix S6100 consumer camera, which was set to a fixed focal length of 28 mm and a size of 4608 by 3456 pixels. Among the 557 images acquired, a subset of 88 pictures was subsequently selected for the construction of the 3D model using SfM (figure 4). To avoid long wave deformations of the 3D model, like cushion or barrel distortions, and to allow for comparisons with future surveys, 35 ground control points (GCP), chosen from among well identified natural targets on the outcrop surface, were surveyed with a Leica TCRA1201+ reflectorless total station from a single station point. For the survey orientation, two vertexes of a baseline linking the station point and a further target point set nearby were successively measured by Relative Rapid Static GNSS positioning techniques in order to georeference the GCPs into the Italian reference system and accurately orient the 3D model connected with them. Among the 35 surveyed GCP, 11 of them were used to constrain the photogrammetric bundle adjustment and for the external orientation of the 3D model, while the remaining 24 allowed for the checking of the metric quality of the obtained model (figure 4). The SfM computations were performed with the Agisoft Metashape program, leading to the production of a dense 3D point cloud consisting of more than 20 million points with an average density of about 19 points/cm^2. The presence of vegetation required a manual cleaning of the

cloud which led to the elimination of over one million points. The final cloud consists of 18,973,380 points (figure 4). The metric quality checks carried out on 20 of the 24 auxiliary GCP showed an average deviation of 18 ± 14 mm on the planimetric component, and of 7 ± 9 mm on the elevation component. The worst results come from GCPs in the periphery (figure 4).

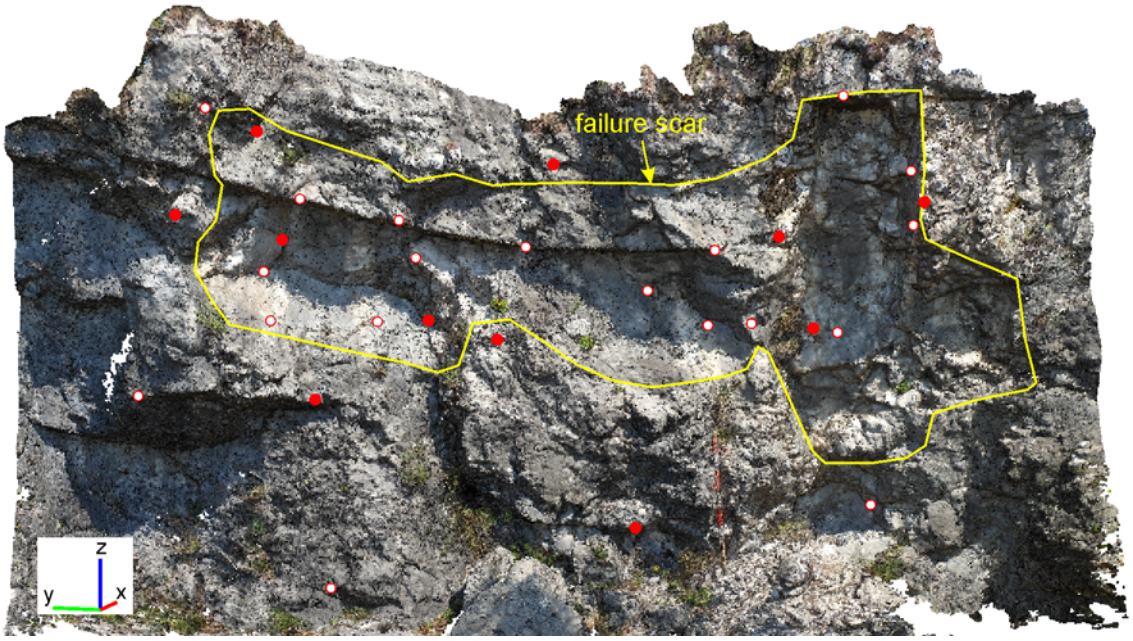

Figure 4. 3D digital model representing the surveyed rock scarp (number of points 18,973,380). The location of the GCP used for the point cloud georeferencing (red dots) and for the post-processing checking (red circled white dots) is also shown. The x-axis points to the north.

In the construction of the 3D digital model of the surveyed rock scarp, particular attention was paid to the effective reproduction of small areas actually corresponding with rock surfaces related to failed rock bridges or gravity-induced joints. Indeed, as demonstrated by field observations, the failed rock bridges can have small surfaces (70–80 cm^2, for the smallest identified), and to properly reproduce them, the 3D point cloud must have a sufficient density. In this manner, the subsequent discontinuity plane extraction and joint orientation calculation can be effective using an adequate software package. Otherwise, an insufficient point cloud density may prevent the identification of these small rock discontinuities, thus preventing a proper geomechanical characterisation of the rock mass, particularly aimed at the identification of possible unstable blocks susceptible to failure. However, when the required detail increases, the calculation time of the point cloud reconstruction increases significantly, passing from a few minutes (lowest detail) up to tens of hours (highest detail), as in our case (9 h). By keeping constant the image set necessary to generate the model, the discriminating parameter is represented by the spatial density of the points you wish to achieve.

To this aim, five different 3D point clouds of various densities were constructed in order to identify a reference threshold value of the point cloud density that allow for the recognition of the failed rock bridges identified on the exposed failure surface of the shallow rockslide (figure 5). As visible in the detailed images of the rock scarp in figure 5, the two failed rock bridges identified on the failure scar (image 1 in figure 5) were not properly reproduced in the point clouds characterised by a density of 0.5 points/cm^2 (image 2) and 2 points/cm^2 (image 3). When constructing a point cloud with density of about 10 points/cm^2 (image 4), the extracted discontinuity planes were not correctly modelled, since their calculated orientations were significantly different when compared with the actual joint orientations measured with the geological compass. For a point cloud density higher than 18 points/cm^2 (images 5 and 6), the failed rock bridge surfaces were properly reconstructed, thus allowing for the calculation of plane orientations very close to the actual joint attitudes.

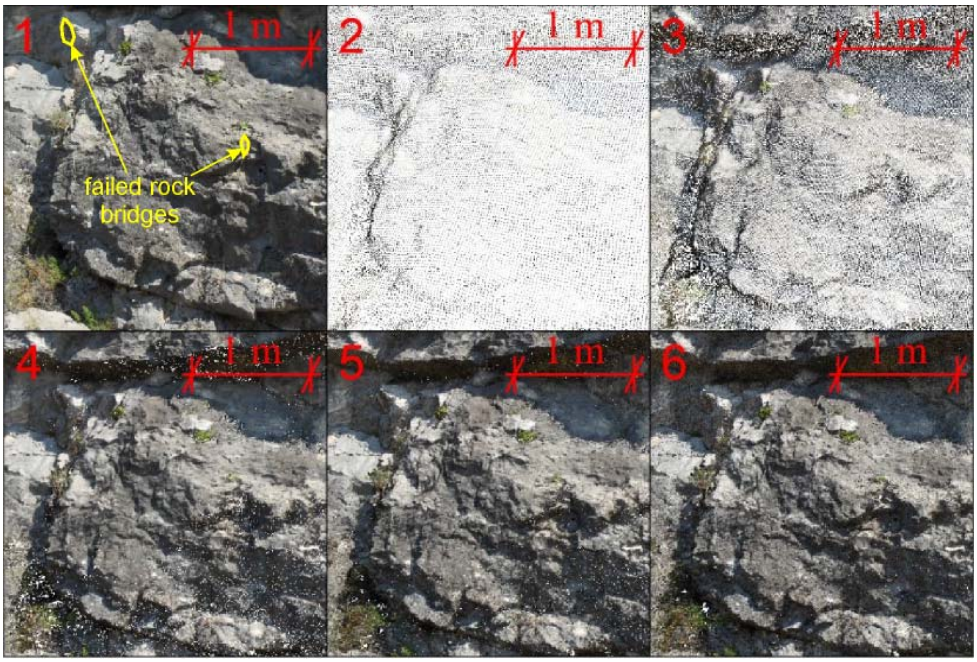

Figure 5. Detail of the slope face showing a comparison between the different values of the point cloud density of the 3D digital model representing the rock outcrop.

5. Joint sets extraction

The dense point cloud representing the 3D digital model of the investigated rock scarp was elaborated in order to extract the rock joint sets by using the software Discontinuity Set Extractor (DSE) [11, 19]. DSE is an open source software that is increasingly used by researchers and professional technicians to identify discontinuity sets affecting rock masses and, for this reason, it was used in the present work. Basically, the methodology adopted in DSE is based on three main steps [20]: (1) a nearest neighbour search aimed at the determination of the plane orientation in each point of the cloud (coplanarity test); (2) a statistical analysis of the planes, consisting in the determination of their average orientations through a kernel density estimation, identifying those points that belong to a same discontinuity set (semi-automatic set identification); and (3) a cluster analysis with localisation of the points defining the different clusters and calculation of the plane equations.

The joint set extraction was confirmed to be strongly sensitive to some controlling parameters embedded in DSE, in particular the *k*-nearest neighbours (*knn*) and the minimum angle between the normal vectors associated with points belonging to different discontinuity sets (*Angle min v ppal*). Figure 6 shows the outcomes of three different extractions performed on the same 3D point cloud, which were carried out assuming different values of *knn* and *Angle min v ppal*. For lower values of *knn* and *Angle min v ppal*, a large number of peaks of relative frequency emerge, but some clusters seem to be split in multiple sets (figure 6a). In this case, the total amount of points that are assigned to a given cluster is higher, but the number of the identified joint sets is clearly overestimated ($N_J = 18$). This problem was solved assuming a higher value of *Angle min v ppal* (figure 6b). In fact, although the pattern of the isolines of relative frequency is the same, the number of the identified joint sets is lower, even if some sets are not associated with clearly highlighted peaks of frequency ($N_J = 11$). Differently, for higher values of *knn* and *Angle min v ppal*, some clusters seem to be merged and are also characterised by a very high variability (figure 6c). In this case, the total amount of points assigned to a given cluster is lower, and the number of the identified joint sets is lower ($N_J = 7$) when compared with previous cases.

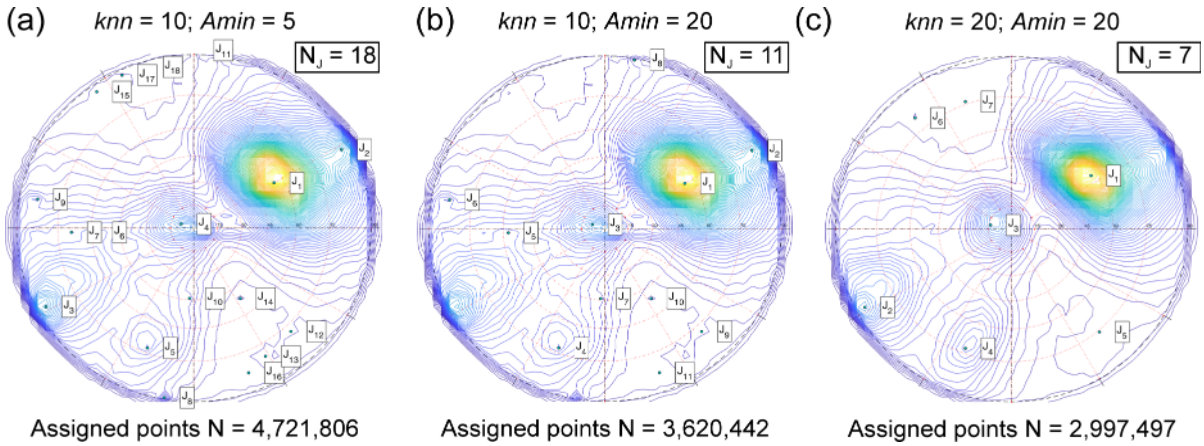

Figure 6. Stereoplot diagrams of extracted joint sets for different values of the controlling parameters embedded in DSE: (a) *knn* = 10 and *Angle min v ppal* = 5 (number of identified sets N_J = 18); (b) *knn* = 10 and *Angle min v ppal* = 20 (N_J = 11); (c) *knn* = 20 and *Angle min v ppal* = 20 (N_J = 7).

6. Discussion and conclusions

It must be noted that, on the basis of the outcomes of the different extractions alone, it is not possible to unambiguously identify the most realistic joint set distribution that represents the actual rock mass arrangement. When performing the joint sets extraction, the sensitivity analysis pointed out the key influence of *knn* and *Angle min v ppal* on the identification of the discontinuity sets. Their values have to be assessed on the basis of the specific case analysed. Therefore, the semi-automatic extraction requires the control of the user in defining the values of the key parameters controlling the analysis. To this end, we performed a comparison between the calculated joint orientation data and the field measurements acquired by means of the geological compass. Notably, the statistical sample of joint measurements collected from the field was found to be significant enough to properly assess the rock mass arrangement. The pole plot of calculated joint planes that best matches the field measurement sample is that obtained assuming *knn* = 10 and *Angle min v ppal* = 20 (figure 7).

When considering the peaks of relative frequency, joint sets J1–J3 have a remarkable resemblance between measured and calculated discontinuity planes (figure 7a, b), even if some small differences emerge in the average attitude and in the specific values of relative frequency of the clusters (figure 7c). Joint sets J4–J6 and J8–J9 have average orientations very close between the two samples, but with the exception of set J9, their frequency peaks are only recognisable in the field measurements (figure 7a). Indeed, the pattern of the isolines of relative frequency in the calculated joint data does not clearly highlight the presence of these discontinuity sets (figure 7b). Joint set J7 was only recognised in the field measurements, since there is no evidence of any peak of relative frequency in the calculated joint planes. In the pole plot distribution of extracted rock joints, three additional sets (J10–J12 in figure 7b) were detected. These sets have a possible resemblance to some areas in the contour pole plot of field measurements (figure 7a), but their relative frequency is lower than 3% (figure 7c). When combining findings from samples of both field measurements and extracted discontinuities, the investigated rock mass is affected by twelve joint sets (J1–J12), including: a few sets with higher relative frequency (15–25%) mainly associated with persistent joints (J1 and J3), numerous sets with a relative frequency ranging from 3% to 9% mainly related to low-continuous joints (J2 and J4–J9), and additional sets (J10–J12) with lower relative frequency (< 3%). This evidence is particularly important, since it demonstrates that sedimentary rock masses can be characterised by a large number of discontinuity sets, which is much higher compared with the typical three joint sets that are commonly considered in geomechanical evaluations of rock masses in order to identify single potentially unstable rock blocks. In fact, these three discontinuity sets are identified on the basis of statistical samples that are not representative of the investigated rock mass, since they include very few field measurements (in most cases, less than 100 measurements).

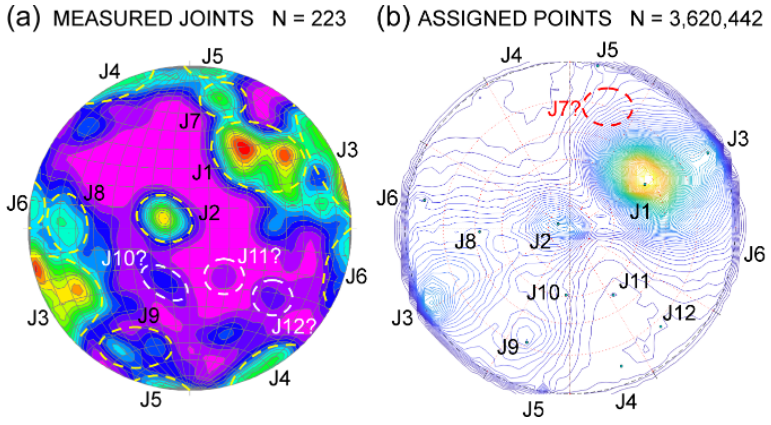

Joint set	Measured joints Dip dir./Dip [°/°]	Rel. freq. [%]	Calculated joints Dip dir./Dip [°/°]	Rel. freq. [%]
J1	227/54	21.5	240/55	20.0
J2	109/14	6.3	108/09	4.4
J3	063/79	23.3	242/87	16.3
J4	338/84	8.5	340/83	1.8
J5	188/85	4.9	190/89	3.5
J6	282/85	5.4	101/84	6.2
J7	194/70	3.6	–	–
J8	095/66	5.8	088/57	5.0
J9	025/71	3.6	021/73	4.8
J10	*029/32*	*2.2*	003/44	2.2
J11	*325/30*	*0.4*	327/51	1.1
J12	*307/60*	*1.3*	317/78	2.0

Figure 7. Pole plots of (a) field measurements, and (b) extracted joint planes. (c) Comparison of average orientations and relative frequencies of measured and calculated discontinuity sets.

On the whole, the analysis carried out in the present study highlights some key issues when adopting a RS approach to identify rock joint sets affecting a rock mass. Firstly, it is necessary to create a 3D point cloud that has a sufficiently high point density to properly reproduce the smallest joint surfaces occurring on the investigated rock face, which are possibly related to the presence of failed intact rock parts. Subsequently, the discontinuity sets extraction from the created 3D point cloud requires a control by the user in order to choose the proper values for the parameters controlling the analysis. However, this control is only effective if the user has a significant statistical sample of joint orientation measurements as reference. When a significant statistical sample of field measurements is lacking (e.g., for inaccessible rock outcrops or due to a scarcity of measurements caused by the laziness of the surveyor), the discontinuity set extraction may be ineffective, since the calculated joint sets cannot be representative of the actual structural arrangement of the rock mass.

In addition, the RS methodology for the assessment of the discontinuity sets affecting a rock mass is able to detect joint planes that are well exposed on the rock face. Differently, fractures that penetrate in the rock mass and are only visible on the rock face as traces cannot be identified (figure 2b). This is caused by the fact that an insufficient number of points of the 3D point cloud is associated with a planar region that satisfies the coplanarity condition tested by common software packages used for the identification of discontinuity planes. This was also found to be true for joints that are orthogonal to the slope face [15], which consequently can be underrated or not properly identified, as for joint set J4 identified in the present study (figure 7c). As a result, gravity-induced joints bounding unstable blocks susceptible to failure remain undetected, thus preventing a proper geomechanical characterisation of the rock mass aimed at the prediction of the potential failure mechanism or slope stability condition. Gravity-induced joints can only be recognised via a field survey performed on the rock outcrop.

For the aforementioned issues, the use of 3D models obtained from RS techniques to identify joint sets affecting unstable rock masses can be very useful in obtaining a large amount of joint orientation data, especially for inaccessible or highly vertically extended outcrops. However, as this work demonstrates, for a comprehensive assessment of the structural arrangement of the investigated rock mass, the exclusive application of a RS approach cannot fully substitute the traditional field survey, and the estimation of discontinuity sets should be integrated with joint orientation measurements acquired using a traditional geological compass. To maximise its capabilities, the semi-automatic discontinuity set extraction from 3D point clouds should always be validated by a significant statistical sample of joint orientation measurements that are preliminarily collected from the field.

References

[1] A. Bolla, and P. Paronuzzi, "Geomechanical field survey to identify an unstable rock slope: The Passo della Morte case history," *Rock Mech. Rock Eng.*, vol. 53, pp. 1521–1544, 2020.

[2] P. Paronuzzi, and A. Bolla, "Gravity-induced fracturing in large rockslides: possible evidence from Vajont," *Engineering Geology for Society and Territory: Landslide Processes*, *Proceedings of the XII International IAEG Congress*, pp. 213–216, 2015.
[3] P. Paronuzzi, and A. Bolla, "Gravity-induced rock mass damage related to large en mass rockslides: evidence from Vajont," *Geomorphology*, vol. 234, pp. 28–53, 2015.
[4] T. Szwedzicki, "Rock mass behaviour prior to failure," *Int. J. Rock Mech. Min. Sci.*, vol. 40, pp. 573–584, 2003.
[5] A. Bolla, and P. Paronuzzi, "Numerical investigation of the pre-collapse behavior and internal damage of an unstable rock slope," *Rock Mech. Rock Eng.*, vol. 53, pp. 2279–2300, 2020.
[6] P. Paronuzzi, and W. Serafini, "Stress state analysis of a collapsed overhanging rock slab: a case study," *Eng. Geol.*, vol. 108, pp. 65–75, 2009.
[7] P. Paronuzzi, A. Bolla, and E. Rigo, "3D Stress-strain analysis of a failed limestone wedge influenced by an intact rock bridge," *Rock Mech. Rock Eng.*, vol. 49, pp. 3223–3242, 2016.
[8] D. Elmo, D. Donati, and D. Stead, "Challenges in the characterisation of intact rock bridges in rock slopes," *Eng. Geol.*, vol. 245, pp. 81–96, 2018.
[9] M. Frayssines, D. Hantz, "Modelling and back-analysing failures in steep limestone cliffs," *Int. J. Rock Mech. Min. Sci.*, vol. 46, pp. 1115–1123, 2009.
[10] M. Sturzenegger, and D. Stead, "Close-range terrestrial digital photogrammetry and terrestrial laser scanning for discontinuity characterization on rock cuts," *Eng. Geol.*, vol. 106, pp. 163–182, 2009.
[11] A. J. Riquelme, A. Abellán, and R. Tomás, "Discontinuity spacing analysis in rock masses using 3D point clouds," *Eng. Geol.*, vol. 195, pp. 185–195, 2015.
[12] W. Xu, Y. Zhang, X. Li, X. Wang, F. Ma, J. Zhao, and Y. Zhang, "Extraction and statistics of discontinuity orientation and trace length from typical fractured rock mass: A case study on the Xinchang underground research laboratory site, China," *Eng. Geol.*, vol. 269, 105553, 2020.
[13] A. J. Riquelme, R. Tomás, and A. Abellán, "Characterization of rock slopes through slope mass rating using 3D point clouds," *Int. J. Rock Mech. Min. Sci.*, vol. 84, pp. 165–176, 2016.
[14] D. Kong, C. Saroglou, F. Wu, and B. Li, "Development and application of UAV-SfM photogrammetry for quantitative characterization of rock mass discontinuities," *Int. J. Rock Mech. Min. Sci.*, vol. 141, 104729, 2021.
[15] N. Menegoni, D. Giordan, C. Perotti, and D. D. Tannant, "Detection and geometric characterization of rock mass discontinuities using a 3D high-resolution digital outcrop model generated from RPAS imagery – Ormea rock slope, Italy," *Eng. Geol.*, vol. 252, pp. 145–163, 2019.
[16] S. Slob, B. Van Knapen, R. Hack, K. Turner, and J. Kemeny, "Method for automated discontinuity analysis of rock slopes with three-dimensional laser scanning," *Transportation Research Record: Journal of the Transportation Research Board; Geology and Properties of Earth Materials*, DOI: 10.3141/1913-18. ISSN: 0361-1981, pp. 187–194, 2005.
[17] A. M. Ferrero, G. Forlani, R. Roncella, and H. I. Voyat, "Advanced Geostructural Survey Methods Applied to Rock Mass Characterization," *Rock Mech. Rock Eng.*, vol. 42, pp. 631–665, 2009.
[18] R. Battulwar, M. Zare-Naghadehi, E. Emami, and J. Sattarvand, "A state-of-the-art review of automated extraction of rock mass discontinuity characteristics using three-dimensional surface models," *J. Rock Mech. Geotech.*, in press, available online.
[19] A. J. Riquelme, "Discontinuity Set Extractor (DSE)," *https://personal.ua.es/en/ariquelme/wiki-dse.html*. Last access date: June 11, 2021.
[20] A. J. Riquelme, A. Abellán, R. Tomás, and M. Jaboyedoff, "A new approach for semi-automatic rock mass joints recognition from 3D point clouds," *Comput. Geosci.*, vol. 68, pp. 38–52, 2014.